Heliyon 10 (2024) e29962

Contents lists available at ScienceDirect

Heliyon

journal homepage: www.cell.com/heliyon

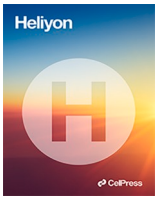

Research article

A new study on the corrosion inhibition mechanism of green walnut husk extract as an agricultural waste for steel protection in HCl solution

Mohammad Akbari Shahmirzadi, Mahboobeh Azadi *

Faculty of Materials and Metallurgical Engineering, Semnan University, Semnan, Iran

ARTICLE INFO

Keywords:
Inhibition mechanism
Steel protection
Corrosion
HCl solution
Green walnut husk extract

ABSTRACT

In this study, green walnut husk (GWH) extract was explored as a cost-effective (waste-agricultural) and eco-friendly inhibitor to increase the corrosion resistance of carbon steel in a 1 M HCl solution. Electrochemical impedance spectroscopy, weight change, and potentiodynamic polarization (PDP) tests were utilized to examine the electrochemical behavior of steel substrates with and without the inhibitor. Atomic force microscopy (AFM), field emission scanning microscopy, Fourier-transform infrared spectroscopy (FTIR), and X-ray diffraction (XRD) were performed to analyze corroded surface structures with and without the inhibitor. This inhibitor was found to be 27–82 % efficient in increasing the corrosion resistance of the steel substrates. When the temperature of the solution was increased from 303 to 323 K, the retardation coefficient decreased due to the physical adsorption of GWH molecules on the surface. The results indicated that GWH acted as a mixed inhibitor, and its adsorption on the surface followed the Langmuir model. AFM measurements showed that the roughness of corroded surfaces decreased by approximately 22 % when the GWH concentration was at its optimum level of 400 ppm. Thermodynamic studies displayed a decrease in the corrosion reaction's activation energy of about 25 %. FTIR and XRD patterns of corroded surfaces represented that hydrated iron chloride was the dominant corrosion product. Furthermore, the results provided insight into the GWH adsorption mechanism.

1. Introduction

A corrosion inhibitor is a chemical substance that, when present in corrosive environments in low concentrations, can effectively reduce or prevent metal corrosion without altering the environment. Hence, using inhibitors is a practical approach to control metallic material corrosion in various industries such as oil and gas exploration, oil refining, chemical processing, and water treatment [1–4]. However, inhibitors are often used mainly in closed environments to choose the appropriate concentration and control their amount easily. Such conditions can be seen in circulating systems, oil production, and refining. Notably, side effects of inhibitors on the environment and the employees' health in the long term result in their application limitation [5–7]. Recently, much attention has been paid to replacing them with nature-friendly materials, novel conducting polymers, nano-materials, and plant or insect extracts have been one of the main areas of research in this field [8–11].

Green organic inhibitors, made up of heterogeneous compounds with oxygen, nitrogen, and sulfur atoms, which are sites for

* Corresponding author.
E-mail address: m.azadi@semnan.ac.ir (M. Azadi).

https://doi.org/10.1016/j.heliyon.2024.e29962
Received 8 February 2024; Received in revised form 17 April 2024; Accepted 18 April 2024
Available online 19 April 2024

absorption on the metal surface [12–14]. Additionally, it is found that plant extracts contain polyphenols, terpenes, alcohols, carboxylic acids, and alkaloids in their main compounds. In this situation, eco-friendly inhibitors can effectively increase the corrosion resistance of steel substrates in the HCl solution. Thus, some recent research was reviewed as follows,

Liao et al. [15] utilized *cocamidopropylamine* oxide as an inhibitor for steel substrate. They found that such a mix-type inhibitor at the critical concentration of 450 ppm exhibited an efficiency of 90 % in 0.5 M HCl solution. Berrissoul et al. [16] evaluated the influence of *Lavandula mairei* extract on the corrosion feature of steel in 1 M HCl solution. Their outcomes showed that the corrosion resistance increased to 88 % when the extract concentration was about 400 ppm. Sajadi et al. [17] studied the properties of *Ranunculus arvensis* and *Glycine* max extracts for mild steel in 1 M HCl solution. They demonstrated that adsorption mechanism for both inhibitors followed by the Langmuir model through physical adsorption. Hassouni et al. [18] indicated that the inhibitor efficiency for extracts of *Origanum elongatum* plant decreased when the temperature increased up to 333 K. Cherrad et al. [19] extracted the oil of *Cupressus arizonica* fruit and showed that the corrosion resistance of carbon steel in the HCl solution would increase when the concentration of the oil raised from 125 to 500 ppm.

In addition, Li et al. [20,21] conducted research on the synergetic effect of potassium iodide, sodium lignosulfonate, and green walnut husk (GWH) for protecting cold rolled steel against corrosion in trichloro-acetic and phosporic acid solutions. Wu et al. [22] considered the effect of GWH on magnesium corrosion in NaCl solution. Therefore, based on the limited research, in this research, as a new study, the GWH extract was used as an abundant, natural, eco-friendly, available, and low-cost inhibitor to reduce corrosion attacks of carbon steel in 1 M HCl solution. GWH is agricultural waste, unlike other extracted green inhibitors in previous studies which were from specific plants, thereby increasing the cost of green inhibitors. Notably, the HCl solution is an appropriate acid medium for acid pickling of steel equipment such as pipes, tubes, and mills. Thus, electrochemical tests were conducted to determine the inhibitor's retardation coefficient in various concentrations. Additionally, thermodynamic and kinetics studies were carried out to identify the optimum inhibitor concentration for st 37 steel to protect it against corrosion. Lastly, based on the obtained experimental results, an adsorption mechanism of GWH extract molecules on the steel surface was suggested.

2. Materials and methods

2.1. Substrate

A steel sheet (st37) with a thickness of 3 mm was used as the substrate. The sheet was cut into a dimension of 1 cm^2. This steel contained 0.16 C, 0.30 Si, 0.41 Mn, and 99.13 % wt Fe. Initially, substrates were ground with sandpaper up to 1200 grit, washed with an acetone solution, and dried at room temperature of 303 K.

2.2. Extraction process

Green walnut husks were collected from walnut trees in Shahmirzad, Iran. They were dried in the open air and then crushed to prepare the inhibitor substance. The produced GWH powder was extracted by Soxhlet extractor in a solution containing 70 % ethanol and 30 % distilled water. The resulting extract was dried in an oven at 50 °C for 15 min. Finally, the powder was ground in a ball-

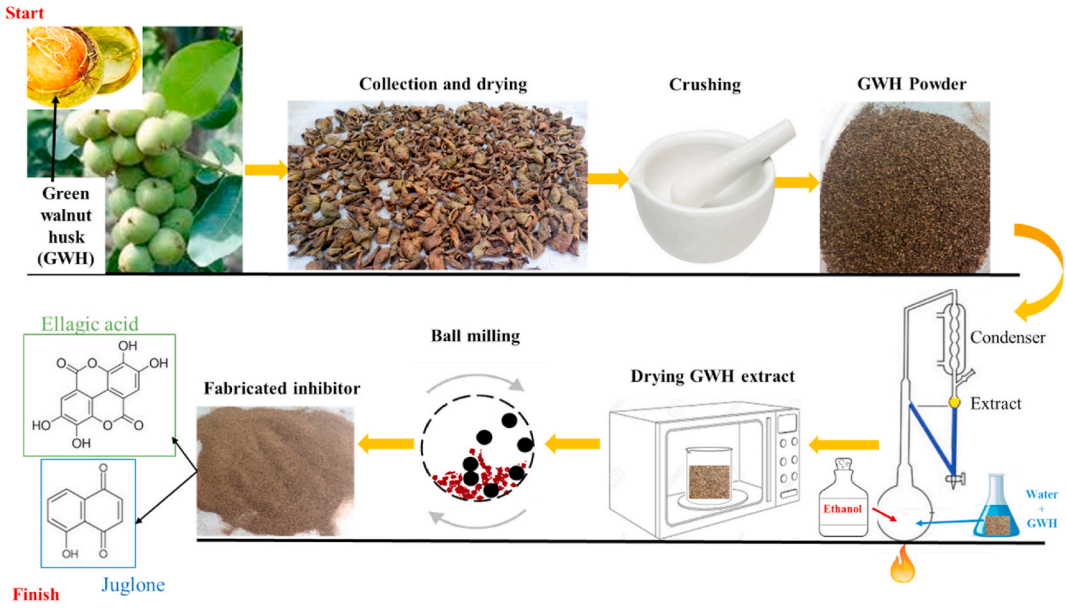

Fig. 1. Schematic of GWH extracting steps and the main chemical composition of green walnut husk (GWH) extract.

milling device to fabricate the inhibitor. The schematic steps of GWH extracting are shown in Fig. 1. Notably, the main chemical composition of the extracted substance was ellagic and juglone acids, as displayed in Fig. 1. However, the GWH consisted of 48.4 % crude fiber, 18.7 % ash, 17.7 % of protein, 6.9 % of lipids, and 8.3 % non-nitrogen components [20,23].

The corrosive media was produced by dilution of HCl (37 %) in distilled water to prepare 1 M HCl solution. To apply the GWH extract, it was added into the corrosive medium in the concentration range of 100–1200 ppm. The extract dissolved completely in the solution up to 800 ppm. However, the insignificant content of the solid was undissolved in concentrations higher than 1000 ppm.

2.3. Electrochemical measurements

Both potentiodynamic polarization (PDP) and electrochemical impedance spectroscopy (EIS) were performed through a potentiostat (Organoflex model) device. A three-electrode system was also operated. A thin sheet of platinum acted as the counter electrode. A saturated calomel electrode (SCE) behaved as the reference rod. An area of 1 cm^2 of the steel sheet was the working electrode. A flat cell was used for both measurements. For Tafel polarization experiments, a DC voltage was utilized with a value of ±250 mV from the open circuit potential (OCP). The scan rate was 0.1 mv s^{-1}. In addition, an AC voltage was applied for EIS tests with a value of ±10 mV from the value of the OCP. The range of the frequency was 10^5 to 10^{-2} Hz. The test temperature was about 30 °C. Notably, before the test, all specimens were immersed in the 1 M HCl solution for 30 min to keep a stable state. The GWH extract concentration range in the corrosive media was about 100–1200 ppm. For studying the adsorption mechanism of GWH extract at steel substrates, equation (1) was used.

$$C/\theta = 1/K_{ads} + C \tag{1}$$

C is the GWH extract concentration, θ is inhibition efficacy (%$R \times 0.01$), and K_{ads} is a constant related to the adsorption equilibrium. Inhibition efficacy formulas were found in other research [24–27].

2.4. Chemical test and thermodynamic studies

Weight change measurements were also done to assess the long-term influence on the inhibition efficacy or the retardation coefficient (%R) of the utilized inhibitor. Thus, the immersion time for such a test was up to 100 h. In this test, the corrosion rate was estimated through equation (2) [14].

$$Corrosion\ rate = \frac{\Delta W}{At} \tag{2}$$

ΔW is the weight change of specimens before and after the immersion in the corrosive solution at specific times, A is the specimen surface area exposed to the solution, and t is the immersion time in the corrosive media.

In addition, three temperatures of 303, 313, and 323 K were used as the test temperature to study the thermodynamic parameters. Therefore, equations (3)–(5) were utilized [22,26],

$$\Delta G^{\circ}_{ads} = -RT\ln\,[1000\ K_{ads}] \tag{3}$$

ΔG°_{ads} is the standard free energy for the adsorption process, T is the solution temperature, and R is the gas constant [28,29].

$$Corrosion\ rate = A\ \exp\left(\frac{-E_a^*}{RT}\right) \tag{4}$$

A is the constant, and E_a^* is the corrosion reaction activation energy for steel substrate in 1 M HCl solution [14,26].

$$\text{Corrosion rate} = \frac{RT}{Nh}\exp\left(\frac{\Delta S^*}{R}\right)\exp\left(\frac{-\Delta H^*}{RT}\right) \tag{5}$$

N is *Avogadro*'s number, h is *Planck*'s constant, ΔS^* is the entropy, and ΔH^* is the enthalpy of the corrosion reaction, respectively.

2.5. Chemical composition investigation

To detect bonds in green walnut husk (GWH), a Fourier-transform infrared spectroscopy (FTIR- Shimadzu 8400S) device was employed. The wavenumber range was about 400–4000 cm^{-1}. In addition, corrosion products were analyzed through this method. X-ray diffraction (XRD-Bruker D8 Advance) was also applied for phase detection of corrosion products resulting from the reaction of the steel substrate in a 1 M HCl solution with and without the GWH extract. The scan rate was about 0.2° min^{-1}. Corrosion products were gathered from the degraded steel surface after 14 days of immersion in the corrosive media.

2.6. Microstructural evaluations

The corroded steel surfaces after 24 h in 1 M HCl with and without the GWH extract were analyzed using field emission scanning electron microscopy (FESEM- Zeiss- Sigma 300 VP). Such a device was appointed with energy-dispersive spectroscopy (EDS). The utilized voltage was 15 kV. Moreover, the surface roughness of the corroded area was evaluated through atomic force microscopy

(AFM- Full Plus- C-2M − FP). The surface scan area was about 12 × 12 μm^2.

3. Results and discussion

3.1. FTIR

The results of FTIR analysis for the GWH extract before and after the drying process are presented in Fig. 2, along with the extracted peaks which are reported in Table 1. It should be noted that no peak disappeared after the drying process, although some peaks had their wavenumber shifted insignificantly. The highest peak was found to be correlated to the O–H bond. Such a finding was consistent with the chemical structure, as reported in Fig. 1. The incomplete filling of Fe's d-orbital with electrons allowed the free electron pair of oxygen to participate in adsorption on the steel substrate, as reported in Refs. [26,27]. Furthermore, the double-bonds of C=O and C=C were found to be sites for the electron accumulation and adsorption at the substrate [30]. These bonds showed peaks at a wavenumber of 1600–1700 cm^{-1}. Peaks at wavenumbers 2918 and 1373 cm^{-1} were attributed to C–H bonds, while those around 600 cm^{-1} were associated with the C–C bond.

3.2. OCP and PDP measurements

Fig. 3(a) presents OCP values during the exposure time for all specimens during a period of 800 s. The OCP values remained relatively stable over time, with a range of approximately −510 to −570 mV. However, the OCP value for the steel substrate without the GWH extract, the value of OCP was more negative than that of other specimens. This indicated that the steel substrate without the inhibitor had a higher thermodynamic propensities undergoing a corrosion reaction compared to the other specimens with the inhibitor. This observation has been noted in other studies as well [24,25]. Since the value of OCP during the exposure remained constant, it could present that no protective or passive layer was formed on the steel substrate [24].

Diagrams of log I as a function of the applied potential (E) at 303 K, representing PDP results for each specimen, are shown in Fig. 3 (b). Moreover, the data extracted from Fig. 3(b) are reported in Table 2, including anodic and cathodic Tafel slopes (β_a and β_c), corrosion potential (E_{corr}), corrosion current density (I_{corr}), and the reduction in current density of the specimen with the GWH extract as compared to the specimen without the inhibitor (% R). The concentration range of GWH extract in 1 M HCl solution was 100–1200 ppm. Upon addition of the GWH extract to the media, the corrosion rates or I_{corr} values for steel specimens significantly reduced. The inhibition efficiency in the presence of GWH extract ranged from 26.2 to 82.0 %. The optimum concentration of GWH extract was 400 ppm, while a higher or lower concentration could cause a reduction in the retardation coefficient. The same behavior was also found in other studies [17,25]. The range of E_{corr} values for specimens with the green inhibitor was −532 to −507 mV. However, E_{corr} for the specimen without the inhibitor was −535 mV. The inhibitor used in the experiment followed as a mixed inhibitor since the change in Ecorr with and without the inhibitor was lower than −85 mV [30]. Additionally, similar to the OCP value, the lowest and most negative value of E_{corr} was related to the steel substrate without the inhibitor, indicating a higher thermodynamics tendency for corrosion reactions. When the GWH extract was added to a 1 M HCl solution, the change in β_a was higher than in β_c, suggesting that the anodic reaction of Fe dissolution ($Fe = Fe^{2+} + 2e^-$) was more affected than the cathodic reaction ($2H^+ + 2e^- = H_2$). Thus, in this situation, inhibitor molecules acted as physical barriers to electron diffusion and movement, thereby reducing the corrosion attack on steel. Notably, Li et al. [20] also reported that the efficiency of GWH extract for steel substrate in 0.1 M Cl_3CCOOH solution was lower than 50 % when the inhibitor concentration decreased to 200 ppm.

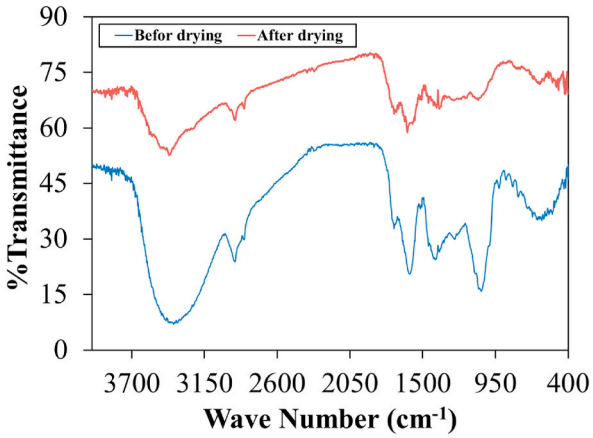

Fig. 2. FTIR patterns for the extract of walnut husk before and after the drying process.

Table 1
Extracted peaks from FTIR patterns in Fig. 2.

Peak position before drying (cm^{-1})	3382	2920	1596	1714	1398	1056	599
Peak position after drying (cm^{-1})	3417	2918	1699	1616	1373	1080	609
Related bond	O–H	C–H	C=O	C=C	C–H	C–O	C–C

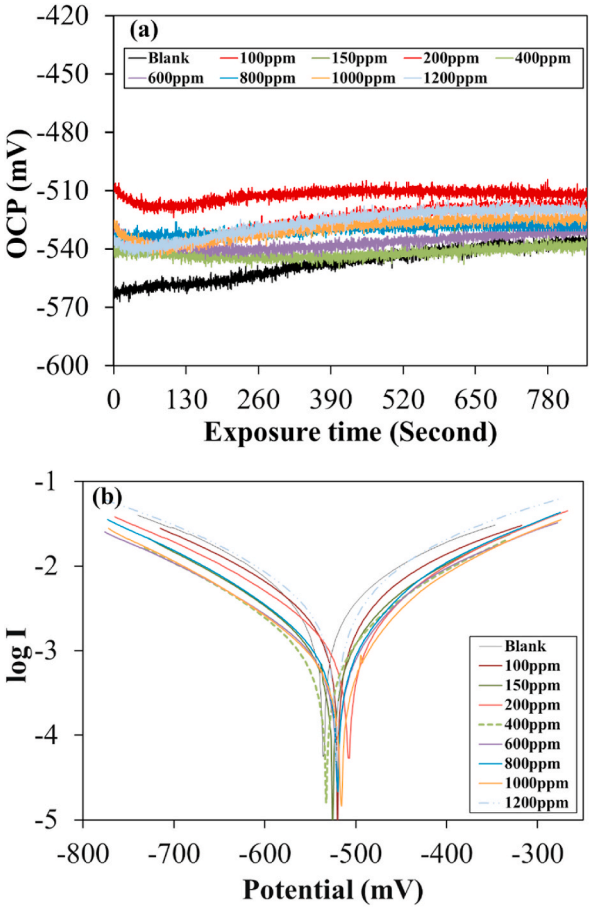

Fig. 3. (a) Diagrams of OCP during the exposure time for various specimens, and (b) diagrams of log *I* versus the potential at 303 K, as results of PDP tests.

Table 2
Extracted data from Fig. 3(b) for PDP measurements.

Inhibitor concentration (ppm)	β_a (mV decade^{-1})	β_c (mV decade^{-1})	E_{corr} (mV)	I_{corr} (mA cm^{-2})	%*R*
0	209	−198	−535	4.4	–
100	186	−205	−519	3.2	27.3
150	136	−171	−525	1.4	68.2
200	114	−152	−507	1.3	70.5
400	99	−146	−520	0.8	82.0
600	101	−137	−520	0.9	79.5
800	131	−180	−516	1.1	75.0
1000	151	−174	−532	1.2	72.3
1200	119	−174	−527	1.5	65.9

3.3. EIS results

The results of EIS test are presented through Nyquist, Bode, and phase angle plots for all specimens at 303 K, as displayed in Fig. 4. Fig. 4(a) illustrates that the shape of the Nyquist diagrams for all specimens, with and without the inhibitor, was the same. However,

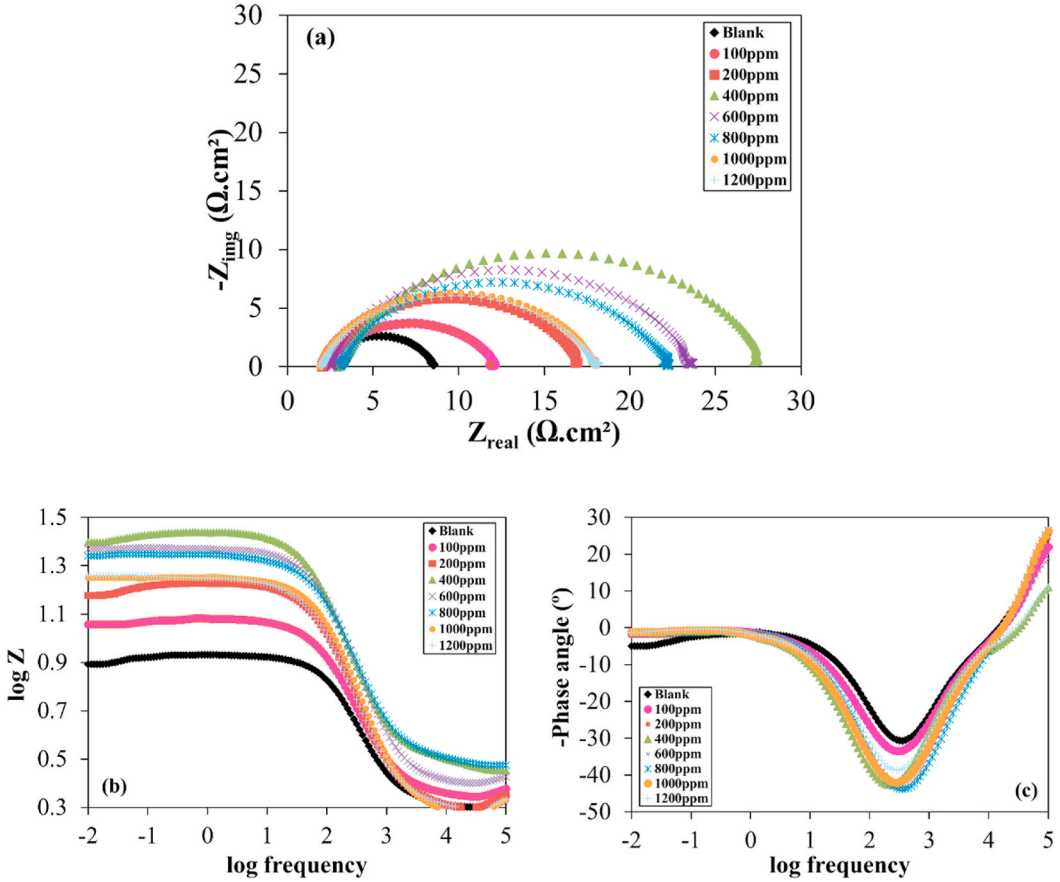

Fig. 4. Diagrams of (a) Nyquist, (b) Bode, and (c) phase angle for various specimens at 303 K.

impedance values increased for specimens with the inhibitor. The Nyquist plots contained a one-semi-ring curve that could show polarization behavior. Fig. 4(b) also describes that impedance modules (*Z*) were higher for specimens with the inhibitor.

The specimen with a 400 ppm concentration of the GWH extract in the corrosive media showed the highest Z value. By increasing the inhibitor concentration from 100 to 400 ppm, values of Z increased. However, increasing the GWH extract concentration from 600 to 1200 ppm, insignificantly decreased the *Z* values. Fig. 4(c) displays that the lowest phase angle was attributed to the mentioned specimen, with a value of −47°. It was noticeable that the minimum peak shifted insignificantly to the lower frequency when the inhibitor was mixed with the corrosive media. The same electrochemical behavior for carbon steel in 1 M HCl solution was also found in other research [19].

To propose a suitable electrical circuit, a ZView software was utilized. The selected circuit for extraction of the EIS data is shown in Fig. 5. It consisted of three components: solution resistance (R_s), polarization resistance (R_p), and a constant phase element for the double-layer (CPE_{dl}). Notably, the capacitor of the double-layer would be changed by *CPE*. Due to micro-inhomogeneity on steel surfaces, the specimens' surface was not entirely flat. To quantify the surface's inhomogeneity, a parameter called "n" was introduced. When the roughness of the steel was high, the value of *n* was close to zero, and whenever the surface roughness was low, *n* became 1 [25]. The same electrical circuit was also found in other studies [27,31].

Table 3 reports the data extracted from EIS measurements. The R_s values for all specimens were about 1.9–3.0 Ω cm^2. This low resistance of the corrosive solution was also observed in other studies [24]. The % *R* shows the increase in polarization resistance of specimens with the GWH extract compared to the specimen without the inhibitor. This value increased as the inhibitor concentration

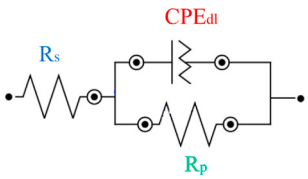

Fig. 5. A suggested circuit for fitting EIS data.

Table 3
Extracted data from EIS measurements.

Inhibitor Concentration (ppm)	R_s (Ω cm^2)	R_p (Ω cm^2)	CPE_{dl} (mF cm^{-2})	n	%R
0	2.1	6.2	0. 33	0.83	–
100	2.3	9.5	0. 33	0.85	34.8
200	2.1	14.4	0. 28	0.86	56.7
400	3.0	24.2	0. 27	0.89	74.2
600	2.6	20.7	0. 21	0.87	70.0
800	1.9	19.5	0. 27	0.87	68.2
1000	2.0	15.6	0. 28	0.86	60.1
1200	2.3	15.5	0. 33	0.85	59.9

increased from 100 to 400 ppm. The range of such increase was about 34.8–74.2 %. The highest R_p value was related to the specimen with the GWH extract at a concentration of 400 ppm. The value of CPE_{dl} was also changed when the inhibitor was added to the corrosive media. For most inhibitor concentrations, the value was lower compared to the blank specimen. Based on the capacity formula [20], the double-layer thickness would increase in the presence of the GWH extract. Additionally, the surface roughness was reduced based on the lower surface area.

The specimen with 400 ppm inhibitor exhibited the highest value for n (0.89) and the lowest surface roughness. This indicates that the corrosion attack was the weakest for this specimen. The metal dissolution caused by the corrosion reaction resulted in a rough surface; however, this was not the case for the specimen with 400 ppm inhibitor. Similar results were reported in other investigations [24–26].

3.4. Weight change measurements

Plots of weight change (WC) versus short exposure time (up to 4 h) at a temperature of 303 K are presented in Fig. 6 (a). The highest

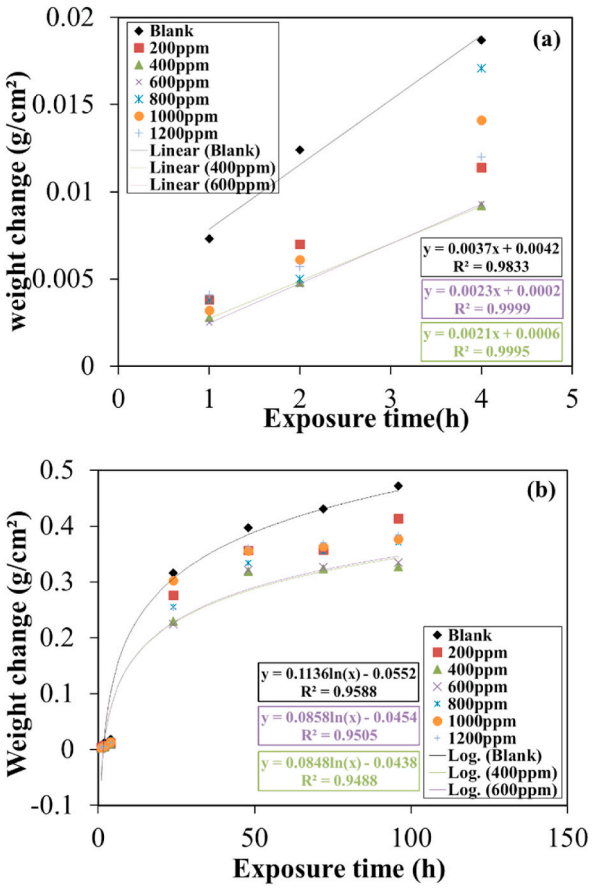

Fig. 6. Plots of weight change (WC) versus the exposure time at a temperature of 303 K (a) for a short time and (b) for a long time of exposure.

weight changes were related to the blank specimen without the inhibitor. However, adding GWH extract to the corrosive media les to a significant decrease in weight changes. The lowest weight change also corresponded to the specimen when the concentration of the inhibitor was 400 ppm. The plot of the slope in Fig. 6 showed the corrosion rate of the specimens [32]. Table 4 shows such data for various specimens. It was notable that based on values of R^2 (the coefficient of correlation [33]) located in Fig. 6(a), weight changes of all specimens versus the time were linear. The range of R values for specimens with the inhibitor was 27.0–43.2 %. R values explained a decrease in the corrosion rate of specimens with the inhibitor compared to specimens without the inhibitor, based on WC data. The effect of a longer time on the corrosion characteristics with and without GWH extract was investigated and the results are as presented in Fig. 6(b).

Similar to Fig. 6(a), the highest and lowest weight changes were attributed to the specimen without and with the inhibitor (with a concentration of 400 ppm), respectively. Notably, the corrosion rate for all specimens increased with the exposure time, indicating that the shelf life of the inhibitor adsorbed on the metal surface decreased with time. In this situation, the detachment of GWH extract from the metallic surface occurred slowly over time. Therefore, the range of R value for specimens with the inhibitor decreased to 13.5–26.9 %. However, based on R^2 values, the plots of the weight change of specimens versus long exposure time followed a logarithmic function.

To investigate the effect of higher temperatures on the retardation coefficient of the GWH extract molecule on the steel surface, the weight change of specimens was measured after a duration of 4 h at temperatures of 313 K and 323 K, as described in Fig. S1. The weight changes were found to increase significantly with increasing temperature. This increase in weight change would result in an increased corrosion rate, as reported in Table 4. The range of R values for steel substrates with inhibitor was 5.6–40.4 %. However, at the temperature of 323 K this range was from 7.5 to 31.0 %. Due to values of R^2, plots of the WC of specimens versus the short exposure time at high temperatures were followed by a linear function.

Fig. 7 displays plots of corrosion rate versus three different temperatures for various specimens. The corrosion rates at 323 K and 313 K were about 3.6–4.9 and 2.4–3.4 times higher compared to the corrosion rate at 303 K, respectively. For all specimens, both with and without the inhibitor, the WC values of specimens obeyed a linear function during short exposure times, based on values of R^2. The highest and lowest corrosion rates for all temperatures corresponded to specimens without and with the inhibitor (at a concentration of 400 ppm), respectively.

3.5. Adsorption mechanism and thermodynamic calculation

Since types of metal surface, corrosive media, and inhibitor molecules were parameters to change the adsorption mechanism, there were many models to describe the adsorption mechanism of inhibitor molecules, such as Langmuir, Temkin, Flowery-Huggins, Bockris-Swinkels, and Frumkin [20,28]. Fig. 8 shows plots of inhibitor concentration (C) compared to the C/θ ratio. When the plot was linear, it demonstrated that the adsorption mechanism of the utilized green inhibitor was Langmuir. Based on the R^2 value for all specimens, it should be noted that the adsorption of GWH molecules on the metallic surface in a 1 M HCl solution followed the Langmuir model. This model assumed that each site on the surface would be occupied by a single inhibitor molecule. Once the critical inhibitor concentration was reached, desorption occurred at a higher concentration. The slopes of plots in Fig. 8 indicated the reverse of (K_{ad}), according to equation (1). Four values of calculated K_{ad} are reported in Table 5, since θ was measured through PDP, EIS, and WC at 303 K. The adsorption free energy (ΔG°_{ad}) was also calculated using equation (2) and is reported in Table 5. The GWH extract molecule adsorption on the metallic surface was determined to be spontaneous. They physically adsorbed on the surface, as the ΔG°_{ad} value was lower than −20 kJ/mol. This meant that the physisorption of inhibitor molecules on the surface would occur. Thus, the inhibitor desorption from the metallic surface at higher temperatures was predictable since in physical adsorption, a weak bond of van der Waals or electrostatic bond was formed between Fe atoms of the surface and organic molecules of the inhibitor. As a result, high temperature resulted in higher activation of GWH extract molecules, and their movement caused desorption from the metal surface. Notably, the same value of ΔG°_{ad} for other green corrosive inhibitors was found for mild steel in 1 M HCl solution [17].

Diagrams of ln (corrosion rate) versus the inverse of temperature for various specimens are displayed in Fig. 9(a). The slope of these plots presented the activation energy (E_a*) as calculated using equation (3). As Table 6 shows, E_a* of the corrosion reaction on the steel surface without the inhibitor was lower than on the surface with the inhibitor. This explained that the rate of corrosion reactions was faster without the inhibitor. However, an increase in E_a* would decrease the corrosion rate of the metallic surface in the presence of the

Table 4
Extracted data based on WC measurements.

Inhibitor Concentration (ppm)	Temperature of 303 K (Short time)		Temperature of 303 K (Long time)		Temperature of 313 K (Short time)		Temperature of 323 K (Short time)	
	Corrosion rate (mg $cm^{-2}h^{-1}$)	%R	Corrosion rate (mg $cm^{-2}h^{-1}$)	%R	Corrosion rate (mg $cm^{-2}h^{-1}$)	%R	Corrosion rate (mg $cm^{-2}h^{-1}$)	%R
0	3.7	–	113.6	–	8.9	–	13.2	–
200	2.5	32.4	99.4	13.5	8.4	5.6	12.2	7.5
400	2.1	43.2	84.8	26.9	5.3	40.4	9.1	31.0
600	2.3	37.8	85.8	25.0	6.8	23.6	10.2	22.7
800	2.5	32.4	97.5	19.2	7.6	14.6	11.4	13.6
1000	2.6	29.7	93.7	17.3	7.7	13.4	11.6	12.1
1200	2.7	27.0	92.6	15.4	7.9	11.2	11.8	10.6

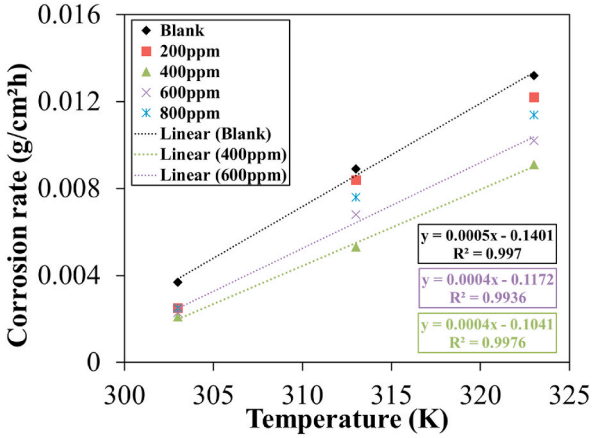

Fig. 7. Plots of corrosion rate versus the temperature for various specimens.

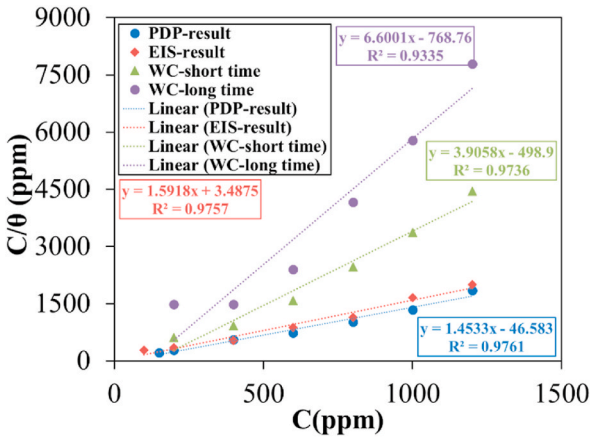

Fig. 8. Plots of C/θ versus C to show the Langmuir adsorption mechanism of the GWH extract based on PDP, EIS, and WC test results.

Table 5
Extracted data from Fig. 8.

	K_{ad} (1/ppm)	ΔG°_{ad} (kJ/mol)
Based on PDP	0.69	−16.45
Based on EIS	0.63	−16.24
Based on WC-short time	0.26	−13.97
Based on WC- long time	0.15	−12.65

GWH extract in the corrosive media. Notably, the increase in values of E_a* by adding the inhibitor was about 15–25 %. Other research has also found a similar trend in E_a* changing with and without the inhibitor [14].

Based on equation (4), the ΔH* and ΔS* of corrosion reactions with and without the GWH extract could be calculated. Thus, in diagrams of ln(corrosion rate/T) versus 1000/T, the plot slope was - ΔH*/2.303R and the intercept was R/Nh + ΔS*/2.303, as represented in Fig. 9(b). The measured values of these two thermodynamic factors are also reported in Table 6. The ΔH* for all corrosion reactions was negative, indicating an exothermic reaction. However, ΔH* values for reactions with the inhibitor were more negative than without the inhibitor. The most negative value of ΔH* was related to the specimen when the concentration of the GWH extract was 400 ppm. Values of ΔS* for reactions with the inhibitor became negative. Such an event showed a higher molecule order at the metal surface. However, the disordering of molecules at the metal surface was high without the inhibitor since ΔS* was a positive value. The value of E_a* was higher than the absolute value of ΔH*, indicating that corrosion reactions were accompanied by a gas evolution. In this case, the production of hydrogen gas is the relevant reaction [9].

Overall, ΔH* was found to be the effective parameter to lower the corrosion rate of steel substrates in 1 M HCl solution with the GWH extract as a green inhibitor. The addition of the inhibitor to the corrosive media led to a change in the value of ΔH* by about 46 %.

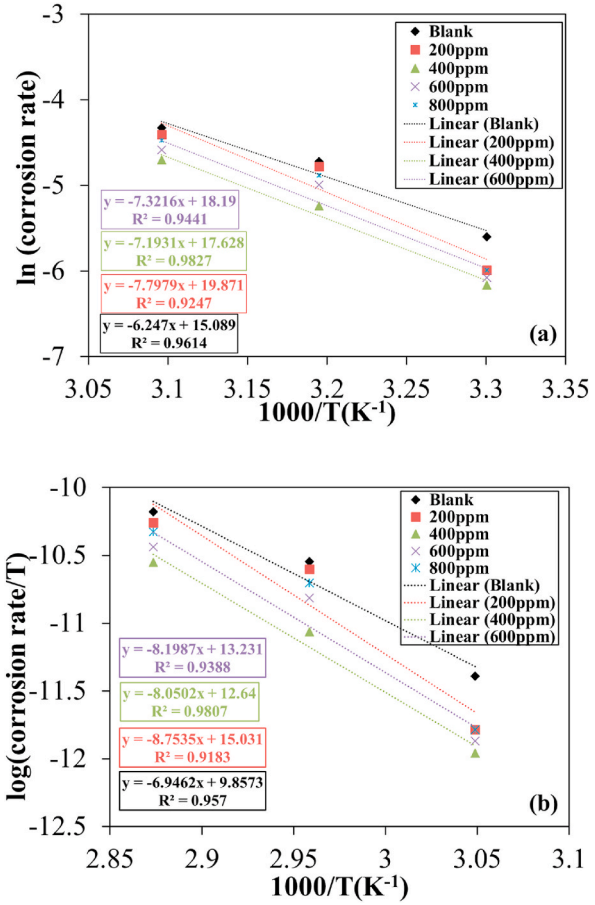

Fig. 9. Diagrams of (a) ln (corrosion rate) versus 1000/*T*, and (b) ln (corrosion rate/*T*) versus 1000/*T* to extract thermodynamic calculations with and without inhibitor.

Table 6
E_a*, ΔS*, and ΔH* values of corrosion reactions for various specimens.

Inhibitor concentration (ppm)	E_a* (kJ/mol)	ΔS* (J/K.mol)	ΔH* (kJ/mol)
0	51.9	3.8	−57.8
200	64.8	−19.3	−83.6
400	59.8	−24.2	−84.6
600	60.9	−39.2	−72.8

3.6. AFM images

AFM images (3D and 2D) of degraded surfaces after 24 h exposure time are represented in Fig. S2. In addition, extracted data from Fig. S2 are summarized in Table 7. The surface roughness of the degraded surface without the inhibitor was higher as compared to the surface with the GWH extract. This observation could show that corrosion attacks were lower when the inhibitor was present in the corrosive media, with a concentration of 400 ppm. The average surface roughness reduction was about 22 % compared to the blank specimen. A similar reduction was also reported in other research papers [24–26].

Table 7
Extracted data from Fig. S2.

Inhibitor concentration (ppm)	Average roughness (nm)	RMS roughness (nm)	Peak to valley roughness (nm)
0	45	61	424
400	35	44	273

3.7. FESEM images

Fig. 10(a–d) reveal the corroded surface of substrates with and without the GWH extract. Corrosion products accumulated on some surface area of the blank specimen and appeared in a protruding shape, as displayed in Fig. 10(a). Moreover, grain boundaries appeared for this specimen after corrosion reactions. Grain boundaries were possible active sites for corrosion attacks compared to grains. In addition, there were some pits on the corroded surface of the specimen without the inhibitor, as shown in Fig. 10(b). However, Fig. 10(c) and (b) explain that when the GWH extract was added to the corrosive solution, accumulated corrosion products decreased, and no pits formed on the corroded surface. In this case, the severity of corrosion attacks decreased based on the GWH extract adsorption on the surface. A similar corroded surface for carbon steel was also found in other research [19,34].

For more details, EDS results (in two modes of map and dot state) are displayed respectively in Fig. 11(a–c) and 12 (a-d), and Table 8, for corroded surfaces after an exposure time of 24 h for the steel substrate with and without the inhibitor. The corrosion products that comprised Fe and O atoms were distributed on the surface homogeneously, as shown in Fig. 11 (b) and (c). However, when the GWH extract was added to the corrosive media, the inhibitor molecules were adsorbed on the corroded surface. This event could be followed by the C element, as presented in Fig. 12 (d).

As reported in Table 8, the amount of O element as a main component of corrosion products on the steel substrate decreased when the corrosive media included the inhibitor. However, the weight percent of the C element, as a component of inhibitor molecules, increased significantly. This observation indicated the adsorption of GWH extract molecules on the surface of the metallic substrate. Notably, the presence of the C element for the corroded surface without the inhibitor was related to the carbon in the steel.

3.8. FTIR results of corroded surfaces

FTIR patterns for corrosion products of metallic substrates without and with the GWH extract in two concentrations of 400 and 600 ppm are presented in Fig. S3. In addition, Table 9 reports extracted peaks from FTIR patterns. There was no significant change in the FTIR pattern for all specimens. However, the intensity of the peak around 3400 cm^{-1} was high when 600 ppm of the GWH extract was added to the corrosive media. Such an event showed the GWH extract adsorption on the surface since the highest peak of GWH extract was found around the mentioned wave number. For selected specimens, two peaks were found for corrosion products. The peak around wavenumber 3400 cm^{-1} was attributed to the hydrated corrosion product of iron chloride. Additionally, a peak around 1650 cm^{-1} could be ascribed to the H_2O molecule adsorption by the Fe substrate. A similar corrosion product was also reported for metallic substrate in the HCl solution [25].

3.9. XRD patterns of corroded surface

Fig. 13 shows XRD patterns of corrosion products for various specimens after 14 days of exposure time. For all specimens, the highest peak at $2\theta = 44^{\circ}$ was related to the Fe phase based on a low thickness of corrosion products collected on the metallic substrate. However, the intensity of such a peak was highest for the specimen without the inhibitor, and such an event indicated a higher corrosion product thickness on the surface. The dominant phase in the corrosion product was FeO (Cl, OH). Moreover, by adding the GWH extract, the height of this peak was remarkably reduced. A similar event was also found in other investigations [25,27]. Other peaks with lower intensity on all specimens have corresponded to α–FeO(OH) and α–Fe_2O_3 phases. When the GWH extract was added to the corrosive media an organic phase of $C_{14}H_{12}O_5$ was also found that was associated with GWH extract molecules. Such an event indicated the inhibitor adsorption on the steel substrate. The same corrosion products were also found for other green inhibitors [25, 28].

3.10. Suggested corrosion inhibition

Based on the obtained results, the suggested inhibition mechanism for steel substrate without and with the GWH extract is schematically represented in Fig. 14. When there was no inhibitor in the corrosive media, ions of the HCl solution and H_2O molecules could be adsorbed on the Fe surface, as arranged in Fig. 14(a). Since Fe had some unfilled D-orbitals from electrons, chloride anions, and H_2O molecules from the oxygen side could be adsorbed on the Fe. Moreover, based on the presence of iron cations on the surface, these anions could move toward the metallic surface. Additionally, based on free electrons of Fe atoms, hydrogen cations were adsorbed on the surface to occur the hydrogen evolution reaction ($2H^+ + 2e^- = H_2$), as the cathodic reaction. In this situation, the total corrosion reaction was mentioned by reaction (1),

$$Fe + 2HCl = FeCl_2 + H_2 \quad (1)$$

However, other possible corrosion reactions would have been done through the following reactions (2–4)

$$Fe.\ H_2O + Cl^- = [FeClOH]^-_{ads} + e^- + H^+ \quad (2)$$

$$[FeClOH]^-_{ads} = FeClOH + e^- \quad (3)$$

$$FeClOH + H^+ = H_2O + Cl^- + Fe^{2+}4) \quad)$$

Thus, the solid corrosion product would be hydrated iron chloride that was unstable in the acidic solution. The same corrosion

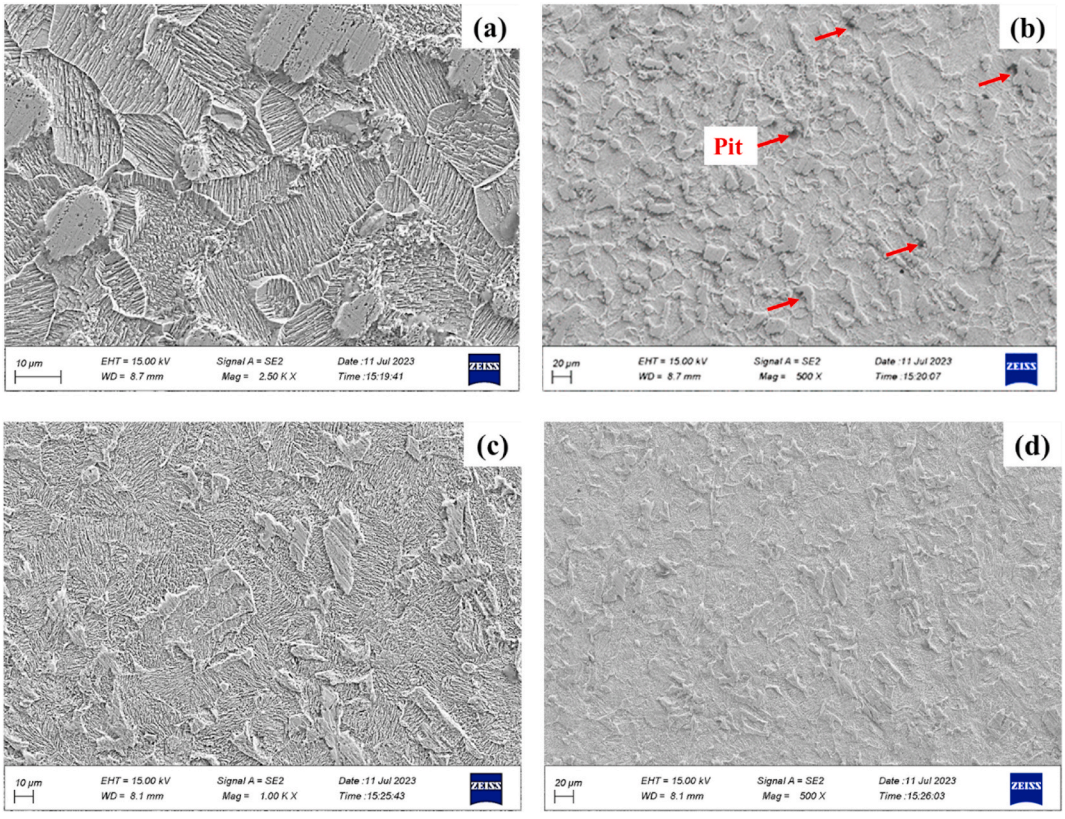

Fig. 10. FESEM images of corroded surfaces after 24 h exposure time (a) and (b) without, and (c) and (d) with the inhibitor.

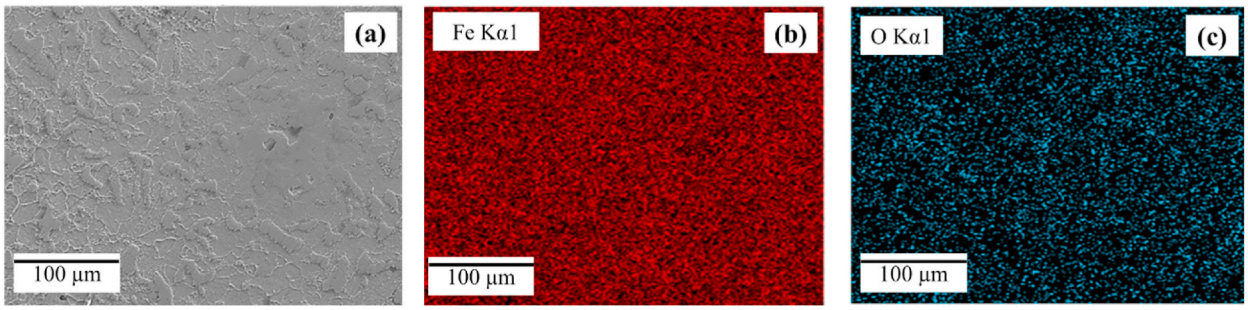

Fig. 11. (a) FESEM images, (b) and (c), Map EDS results for the corroded surface after 24 h exposure time for the steel substrate without the inhibitor, contained Fe and O elements.

mechanism was also found in other research [35–37].

However, when the GWH extract was present in the corrosive media, the reaction (5) would also happen.

$$[GWH]_{sol} + [H_2O]_{ads} = [GWH]_{ads} + [H_2O]_{sol} \quad (5)$$

In this case, H_2O molecules desorbed from the Fe surface when GWH extract molecules were physically adsorbed on the metallic surface. Fig. 14(b) demonstrates this. The GWH extract molecules were able to get adsorbed through the cyclic carbon group and oxygen in their structure towards the Fe surface due to their accumulated electrons (Fig. 14(c)). When the GWH extract molecules reached the metal surface, they acted as barriers for other species like hydrogen cations, which slowed down the reduction reaction. In this manner, the carbon steel corrosion rate would be significantly reduced.

4. Conclusions

In this research, the inhibitory efficiency of GWH extract against the corrosion of carbon steel in 1 M HCl solution was evaluated.

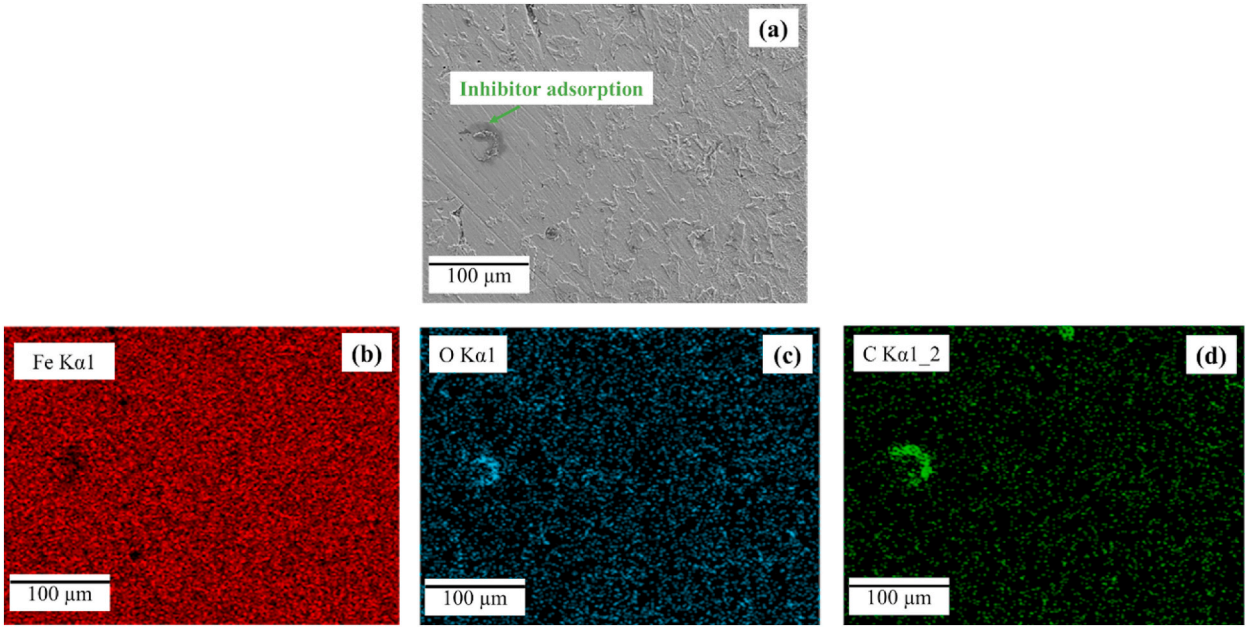

Fig. 12. (a) FESEM images, (b), (c) and (d) Map EDS results (contained Fe, O, and C elements, respectively) for the corroded surface after 24 h exposure time for the steel substrate with the GWH extract when the inhibitor concentration was 400 ppm.

Table 8
Weight and atomic percent of elements on corroded surfaces after 24 h (a) without, and (b) with the inhibitor.

Elements	Weight %	Atomic %	Elements	Weight %	Atomic %
Fe	91.3	81.0	Fe	84.7	58.0
O	4.9	11.2	O	3.6	8.6
C	1.5	4.5	C	9.6	30.9
Cl	2.3	3.3	Cl	2.1	2.5

Table 9
Extracted peaks from FTIR patterns in Fig. S3.

Peak position for blank(cm^{-1})	Peak position for 400- ppm(cm^{-1})	Peak position for 600- ppm (cm^{-1})	Related bonds
3398.34	3419.56	3431.13	Fe–Cl (O–H)
1649.07	1647.09	1649.02	H_2O

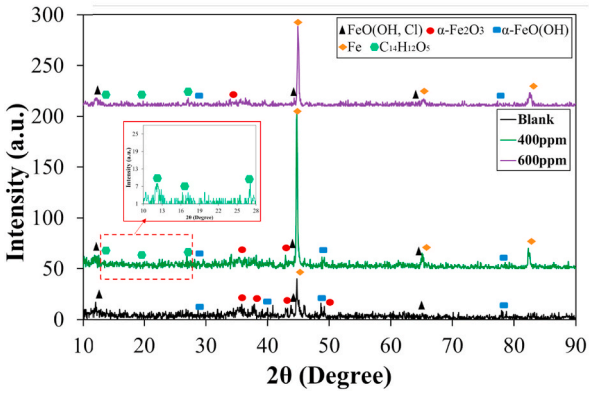

Fig. 13. XRD patterns of corrosion products for various specimens.

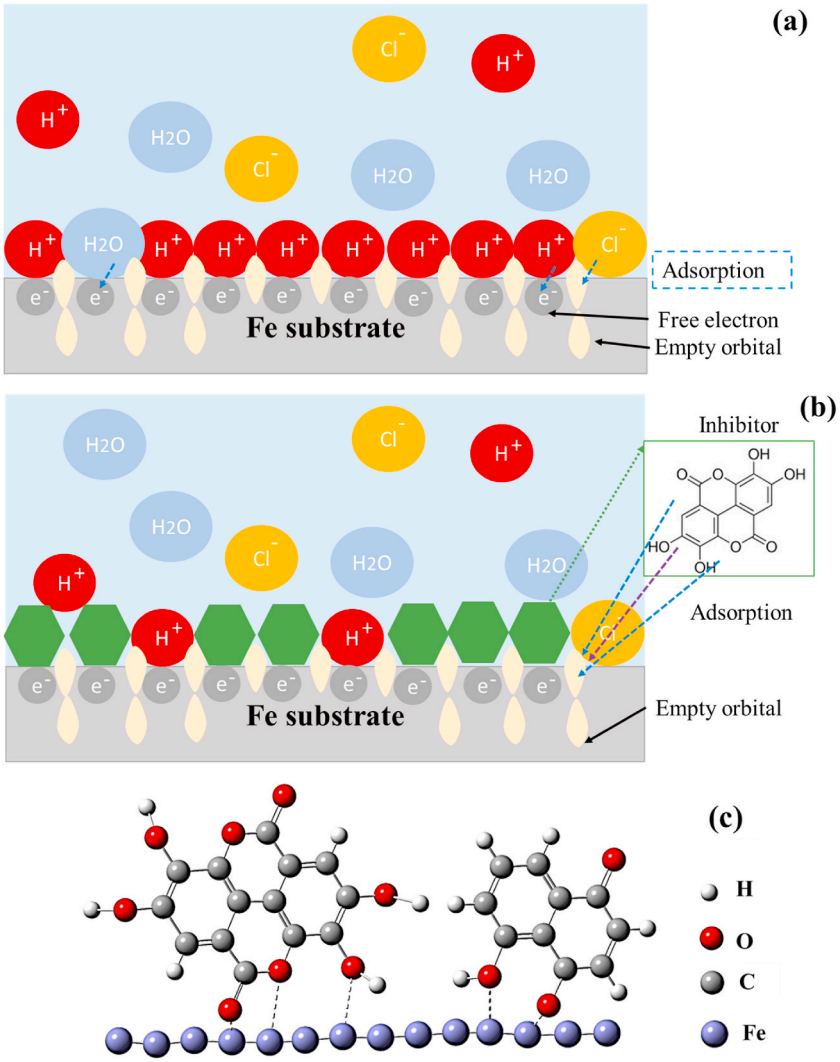

Fig. 14. Schematic images of molecular adsorption at the steel substrate surface in the HCl solution (a) without, (b), and (c) with the GWH extract.

The study found that the inhibitor's efficiency improved to 82 % when the GWH extract concentration increased to 400 ppm, and the temperature was reduced to 303 K. However, increasing the GWH extract concentration to 1200 ppm could lead to a reduction in the inhibitor's efficiency to 65 %. The adsorption of the extracted GWH molecules on the carbon steel was controlled by the Langmuir isotherm mechanism, and the adsorption mode was physical. The addition of GWH extract to the solution increased the activation energy of corrosion reactions by 15–25 %. However, the change in the enthalpy value was about 46 % when the inhibitor concentration was 400 ppm. The images obtained through FESEM and AFM techniques have confirmed that the inhibitor formed a barrier layer, which resulted in a significant decrease in the roughness of the surface. about 22 %.

Data availability statement

Data will be made available on request.

CRediT authorship contribution statement

Mohammad Akbari Shahmirzadi: Methodology, Investigation, Data curation. **Mahboobeh Azadi:** Writing – review & editing, Writing – original draft, Supervision, Data curation.

Declaration of competing interest

The authors declare that they have no known competing financial interests or personal relationships that could have appeared to

influence the work reported in this paper.

Appendix A. Supplementary data

Supplementary data to this article can be found online at https://doi.org/10.1016/j.heliyon.2024.e29962.

References

[1] A.O. Alao, A.P. Popoola, M.O. Dada, O. Sanni, Utilization of green inhibitors as a sustainable corrosion control method for steel in petrochemical industries: a review, Front. Energy Res. 10 (2023) 1063315.
[2] M. Benarioua, A. Mihi, N. Bouzeghaia, M. Naoun, Mild steel corrosion inhibition by Parsley (Petroselium Sativum) extract in acidic media, Egyptian Journal of Petroleum 28 (2019) 155–159.
[3] K. Raviprabha, R.S. Bhat, 5-(3-Pryridyl)-4H-1,2,4-triazole-3-thiol as potential corrosion inhibitor for aa6061 aluminium alloy in 0.1 m hydrochloric acid solution, Surf. Eng. Appl. Electrochem. 55 (2019) 723–733.
[4] K. Raviprabha, R.S. Bhat, Electrochemical and quantum chemical studies of 5-[(4-chlorophenoxy) methyl]-4h-1,2,4-triazole-3-thiol on the corrosion inhibition of 6061 Al alloy in hydrochloric acid, J. Fail. Anal. Prev. 20 (2020) 1598–1608.
[5] C.A.R. Maestro, A.M.S. Malafaia, C.F. Silva, C.S. Nascimento, K.B. Borges, T.A. Simoes, V.R. Capelossi, A.H.S. Bueno, Corrosion resistance improvement of mild steel in different pH using peel garlic green inhibitor, Mater. Chem. Phys. 305 (2023) 127971.
[6] K.O. Shamsheera, A.R. Prasad, M. Arshad, A. Joseph, A sustainable method of mitigating acid corrosion of mild steel using jackfruit pectin (JP) as green inhibitor: theoretical and electrochemical studies, J. Indian Chem. Soc. 99 (1) (2022) 100271.
[7] K. Raviprabha, R.S. Bhat, Inhibition effects of ethyl-2-amino-4-methyl-1,3-thiazole-5-carboxylate on the corrosion of AA6061 alloy in hydrochloric acid Media, J. Fail. Anal. Prev. 19 (2019) 1464–1474.
[8] V. Vorobyova, M. Sakiba, E. Gnatko, Agri-food wastes extract as sustainable-green inhibitors corrosion of steel in sodium chloride solution: a close look at the mechanism of inhibiting action, S. Afr. J. Chem. Eng. 43 (1) (2023) 273–295.
[9] A.H. Al-Moubaraki, S.D. Al-Malwi, Experimental and theoretical evaluation of aqueous black mustard seeds extract as sustainable-green inhibitor for mild steel corrosion in H_2SO_4 acid solutions, J. Adhes. Sci. Technol. 36 (2022) 23–24.
[10] S. Bhaskara, S. Pathapalya Fakrudeen, V. Bheema Raju, H.C. Ananda Murthy, A.V. Raghu, Comparative studies of inhibitive effects of diamines on corrosion of aluminium alloy in presence of acid media, RASAYAN Journal of Chemistry (2021) 72–82.
[11] R. Prabhu, B. Roopashree, T. Jeevananda, S. Rao, K. Raghava Reddy, A.V. Raghu, Synthesis and corrosion resistance properties of novel conjugated polymer-$Cu_2Cl_4L_3$ composites, Materials Science for Energy Technologies 4 (2021) 92–99.
[12] K. Kannan, D. Radhika, A.S. Nesaraj, K. Kumar Sadasivuni, K. Raghava Reddy, D. Kasai, A.V. Raghu, Photocatalytic, antibacterial and electrochemical properties of novel rare earth metal oxides-based nanohybrids, Materials Science for Energy Technologies 3 (2020) 853–861.
[13] M. Rassouli, M. Azadi, Parasites as metal corrosion inhibitors, new achievements, Current Green Chemistry 10 (2) (2023) 105–108.
[14] H.S. Gadow, M. Fakeeh, Green inhibitor of carbon steel corrosion in 1 M hydrochloric acid: eruca sativa seed extract (experimental and theoretical studies), RSC Adv. 12 (2022) 8953–8986.
[15] L.L. Liao, S. Mo, J.L. Lei, H.Q. Luo, N.B. Li, Application of a cosmetic additive as an eco-friendly inhibitor for mild steel corrosion in HCl solution, J. Colloid Interface Sci. 474 (2016) 68–77.
[16] A. Berrissoul, A. Ouarhach, F. Benhiba, A. Romane, A. Zarrouk, A. Guenbour, B. Dikici, A. Dafali, Evaluation of Lavandula mairei extract as green inhibitor for mild steel corrosion in 1 M HCl solution. Experimental and theoretical approach, J. Mol. Liq. 313 (2020) 113493.
[17] G.S. Sajadi, R. Naghizade, L. Zeidabadinejad, Z. Golshani, M. Amiri, S.M.A. Hosseini, Experimental and theoretical investigation of mild steel corrosion control in acidic solution by Ranunculus arvensis and Glycine max extracts as novel green inhibitors, Heliyon 8 (2022) 10983.
[18] H.E. Hassouni, A. Elyousfi, F. Benhiba, N. Setti, A. Romane, T. Benhadda, A. Zarrouk, A. Dafali, Corrosion inhibition, surface adsorption and computational studies of new sustainable and green inhibitor for mild steel in acidic medium, Inorg. Chem. Commun. 143 (2022) 109801.
[19] S. Cherrad, A.A. Alrashdi, H.S. Lee, Y. El aoufir, H. Lgaz, B. Satrani, M. Ghanmi, E.M. Aouane, A. Chaouch, Cupressus arizonica fruit essential oil: a novel green inhibitor for acid corrosion of carbon steel, Arab. J. Chem. 15 (2022) 103849.
[20] X. Li, S. Deng, Synergistic inhibition effect of walnut green husk extract and potassium iodide on the corrosion of cold rolled steel in trichloroacetic acid solution, J. Mater. Res. Technol. 9 (6) (2020) 15604–15620.
[21] X. Li, S. Deng, G. Du, X. Xie, Synergistic inhibition effect of walnut green husk extract and sodium lignosulfonate on the corrosion of cold rolled steel in phosphoric acid solution, J. Taiwan Inst. Chem. Eng. 114 (2020) 263–283.
[22] Y. Wu, Y. Zhang, Y. Jiang, N. Li, Y. Zhang, L. Wang, J. Zhang, Exploration of walnut green husk extract as a renewable biomass source to develop highly effective corrosion inhibitors for magnesium alloys in sodium chloride solution: integrated experimental and theoretical studies, Colloids Surf. A Physicochem. Eng. Asp. 626 (2021) 126969.
[23] A. Jahanban-Esfahlan, A. Ostadrahimi, M. Tabibiazar, R. Amarowicz, A comprehensive review on the chemical constituents and functional uses of walnut (juglans spp.) husk, Int. J. Mol. Sci. 20 (16) (2019) 3920.
[24] M.A. Bidi, M. Azadi, M. Rassouli, Comparing the inhibition efficiency of two bio-inhibitors to control the corrosion rate of carbon steel in acidic solutions, Analytical and Bioanalytical Electrochemistry 13 (1) (2021) 52–66.
[25] H. Mobtaker, M. Azadi, M. Rassouli, The corrosion inhibition of carbon steel in 1 M HCl solution by Oestrus ovis larvae extract as a new bio–inhibitor, Heliyon 8 (12) (2022) 12297.
[26] M.A. Bidi, M. Azadi, M. Rassouli, An enhancement on corrosion resistance of low carbon steel by a novel bio-inhibitor (leech extract) in the H2SO4 solution, Surface. Interfac. 24 (2021) 101159.
[27] H. Mobtaker, M. Azadi, N. Hassani, M. Neek-Amal, M. Rassouli, M.A. Bidi, The inhibition performance of quinoa seed on corrosion behavior of carbon steel in the HCl solution; theoretical and experimental evaluations, J. Mol. Liq. 335 (2021) 116183.
[28] B. Jafari, M. Yousefpour, M. Azadi, The inhibition effect of white dextrin on Al1050 alloy corrosion behavior in the NaOH media: thermodynamic and kinetic study, J. Indian Chem. Soc. 100 (10) (2023) 101089.
[29] K. Raviprabha, R.S. Bhat, Corrosion inhibition of mild steel in 0.5 M HCl by substituted 1,3,4-oxadiazole, Egyptian Journal of Petroleum 32 (2) (2023) 1–10.
[30] M.A. Bidi, M. Azadi, M. Rassouli, A new green inhibitor for lowering the corrosion rate of carbon steel in 1 M HCl solution: hyalomma tick extract, Mater. Today Commun. 24 (2020) 100996.
[31] M. Shkoor, R. Jalab, M. Khaled, T.S. Shawkat, H.M. Korashy, M. Saad, H.L. Su, A.D. Bani-Yaseen, Experimental and theoretical investigations of the effect of bis-phenylurea-based aliphatic amine derivative as an efficient green corrosion inhibitor for carbon steel in HCl solution, Heliyon 9 (2023) 20254.
[32] M. Arab, M. Azadi, O. Mirzaee, Effects of manufacturing parameters on the corrosion behavior of Al–B4C nanocomposites, Mater. Chem. Phys. 253 (2020) 123259.
[33] M. Azadi, M. Ferdosi Heragh, M.A. Bidi, Electrochemical characterizations of epoxy coatings embedded by modified calcium carbonate particles, Progress in Color, Colorants and Coatings 13 (4) (2020) 213–222.

[34] M. Rehioui, S. Abbout, B. Benzidia, H. Hammouch, H. Erramli, N.A. Daoud, N. Badrane, N. Hajjaji, Corrosion inhibiting effect of a green formulation based on Opuntia Dillenii seed oil for iron in acid rain solution, Heliyon 7 (2021) 06674.
[35] S.E. Nataraja, T.V. Venkatesha, H.C. Tandon, Computational and experimental evaluation of the acid corrosion inhibition of steel by tacrine, Corrosion Sci. 60 (2012) 214–223.
[36] B. Liao, Shiquan Ma, S. Zhang, X. Li, R. Quan, S. Wan, X. Guo, Fructus cannabis protein extract powder as a green and high effective corrosion inhibitor for Q235 carbon steel in 1 M HCl solution, Int. J. Biol. Macromol. 239 (2023) 124358.
[37] Q. Wang, Q. Zhang, L. Liu, H. Zheng, X. Wu, Z. Li, P. Gao, Y. Sun, Z. Yan, X. Li, Experimental, DFT and MD evaluation of Nandina domestica Thunb. extract as green inhibitor for carbon steel corrosion in acidic medium, J. Mol. Struct. 1265 (2022) 133367.